

The C-terminus SH3-binding domain of Kv1.3 is required for the actin-mediated immobilization of the channel via cortactin

Peter Hajdu^{*}, Geoffrey V. Martin^{*}, Ameet A. Chimote^{*}, Orsolya Szilagyi^{*,#}, Koichi Takimoto[¥] and Laura Conforti^{*}

^{*}: Division of Nephrology and Hypertension, Department of Internal Medicine, University of Cincinnati, Cincinnati OH 45267

[¥]: Department of Bioengineering and Bioinformatics, Nagaoka University of Technology, Nagaoka, Japan

[#]: Department of Biophysics and Cell Biology, University of Debrecen, Debrecen, Hungary,

Corresponding author:

Laura Conforti
Department of Internal Medicine
Division of Nephrology and Hypertension
231 Albert Sabin Way
University of Cincinnati
Cincinnati, OH 45267-0585
Phone # (513) 558-6009
Fax # (513) 558-4309
Email address: laura.conforti@uc.edu

Running head: Kv1.3 membrane mobility

Abbreviations: APC: antigen presenting cell, EGFP: enhanced green fluorescent protein, FRAP: fluorescent recovery after photobleaching, SLE: systemic lupus erythematosus, HS1: hematopoietic lineage cell-specific protein, PSD-95: postsynaptic density protein 95, hDlg1: human discs, large homolog 1 protein, SH3: SRC homology 3 domain, EGTA: ethylene glycol tetraacetic acid, *HEPES*: 4-(2-hydroxyethyl)-1-piperazineethanesulfonic acid, HEK-293: human embryonic kidney cell line 293, shRNA: short hairpin RNA, PLA: proximity ligation assay, CD: cluster of differentiation

ABSTRACT

Kv1.3 channels play a pivotal role in the activation and migration of T lymphocytes. These functions are accompanied by the channels' polarization which is essential for associated downstream events. However, the mechanisms that govern the membrane movement of Kv1.3 channels remain unclear. F-actin polymerization occurs concomitantly to channels' polarization implicating the actin cytoskeleton in this process. Here we show that cortactin, a factor initiating actin network, controls the membrane mobilization of Kv1.3 channels. FRAP with EGFP-tagged Kv1.3 channels demonstrate that knocking down cortactin decreases the actin-based immobilization of the channels. Using various deletion and mutation constructs, we show that

the SH3 motif of Kv1.3 mediates the channel immobilization. Proximity ligation assays indicate that deletion or mutation of the SH3 motif also disrupts interaction of the channel with cortactin. In T lymphocytes, the interaction between HS1 (the cortactin homologue) and Kv1.3 occurs at the immune synapse and requires the channel's C-terminal domain. These results show that actin dynamics regulates the membrane motility of Kv1.3 channels. They also provide evidence that the SH3 motif of the channel and cortactin play key roles in this process.

INTRODUCTION

The ability of membrane proteins to compartmentalize in specific membrane domains is essential to cell function. This is particularly true for T lymphocytes which polarize when they migrate and activate. Activation of T lymphocytes is initiated by the encounter with antigen presenting cells (APC). The physical interaction between the T cell and the APC leads to a cascade of cellular events including polarization of the T cell with accumulation of cell surface proteins, intracellular organelles, and signaling molecules at the T-APC contact site, forming a highly organized signaling zone known as the immunological synapse (IS) (Cahalan and Chandy, 2009; Kummerow *et al.*, 2009). The movement of specific cell surface proteins into the IS is necessary for proper activation of the T cell as disruption of the IS architecture can lead to either T cell hypo- or hyper activation (Mossman *et al.*, 2005).

One important cell surface protein that localizes to the IS during T cell activation is the voltage-gated potassium channel, Kv1.3. Kv1.3 channels play an essential role in the T cell activation process by regulating the electrochemical driving force for Ca^{2+} influx and generation of the intracellular Ca^{2+} concentration ($[\text{Ca}^{2+}]_i$) necessary for downstream transcription factor activation and T cell clonal expansion (Wulff *et al.*, 2003; Hu *et al.*, 2013). Indeed, blocking Kv1.3 channel's current suppresses Ca^{2+} influx and T cell activation (Cahalan and Chandy, 2009; Hajdu *et al.*, 2013). Furthermore, improper localization of Kv1.3 to the IS leads to altered $[\text{Ca}^{2+}]_i$ dynamics, and has been associated with aberrant T cell signaling in systemic lupus erythematosus (SLE) (Nicolaou *et al.*, 2007; Nicolaou *et al.*, 2009; Nicolaou *et al.*, 2010). The exact mechanisms governing the movement of Kv1.3 to the IS and the channel's accumulation at this site are not fully understood, although it has been shown that membrane-incorporated Kv1.3 proteins move into the IS via lateral movement along the plane of the plasma membrane (Nicolaou *et al.*, 2009). The processes by which proteins gather at the IS are in general still poorly understood. Synapse organization has often been said to involve the phenomenon of "diffusion trapping" which depends on both passive (molecular diffusion) and active mechanisms (involving the actin cytoskeleton) (Favier *et al.*, 2001; Douglass and Vale, 2005; Davis and van der Merwe, 2006; Dushek *et al.*, 2008). The actin cytoskeleton has been implicated in the transport and trapping at the IS of various proteins including the TCR (Dustin, 2007; Dushek *et al.*, 2008; Babich *et al.*, 2012). Several studies reported that association of channels of the Kv1 family to actin is guaranteed by adapter proteins which possess actin-binding domains: PDZ-binding proteins, like hDlg1 (disc large 1), and cortactin. The binding of cortactin and PDZ proteins to Kv channels occurs at the C-terminal region of the channel with cortactin binding associated with a 19 amino acid long sequence in Kv1.2 channels and PDZ binding occurring at a TDV amino acid motif in Kv1.3 and Kv1.4 channels (Imamura *et al.*, 2002; Marks and Fadool, 2007; Doczi *et al.*, 2011). Additionally, the Src homology 3 (SH3) domain, which can be found on cortactin, PDZ proteins, and Kv channels, may also play a role in

these proteins' interactions as SH3 binding domains have been found to be integral in PDZ protein induced clustering of Kv1.4, and have been associated with modulation of Kv1.3 current (Shin *et al.*, 2000; Marks and Fadool, 2007). T cells express the cortactin analog HS1 (hematopoietic lineage cell-specific protein 1) and the PDZ binding proteins hDlg1 and PSD-95 which are able to form complexes with actin and bind multiple Kv channel isoforms (Daly, 2004; Xavier *et al.*, 2004; Carrizosa *et al.*, 2009). HS1 in T cells was shown to be necessary for the accumulation of F-actin to the IS, and for the development of the appropriate signaling post IS formation (Gomez *et al.*, 2006). Furthermore, C-terminal truncation of Kv1.3 or knockdown of PSD-95 in Jurkat T cells has been recently reported to decrease the amount of Kv1.3 channels in the IS at early time points (Szilágyi *et al.*, 2013). Thus, it is possible that the interaction with actin drives and stabilizes Kv1.3 compartmentalization to the IS. Nevertheless, the involvement of the aforementioned proteins in actin-mediated Kv1.3 membrane motility remains unclear. In the present study, wild-type Kv1.3 channels and C-terminal mutated Kv1.3 channels lacking cortactin, SH3 or PDZ binding motifs were investigated to further elucidate the mechanisms and the molecular requirements for Kv1.3 lateral membrane mobility and localization.

RESULTS

Co-localization of Kv1.3 channels with cortactin

It was described that cortactin has a Kv channel binding sequence and binds to various ion channels (Hattan *et al.*, 2002; Tian *et al.*, 2006; Williams *et al.*, 2007; Cheng *et al.*, 2011; Ilatovskaya *et al.*, 2011; Herrmann *et al.*, 2012). Thus, to reveal whether Kv1.3 channels co-localize with cortactin, we performed immunocytochemistry experiments using a HEK-293 cell line which stably expresses FLAG-Kv1.3 channels. We labeled the plasma membrane localized Kv1.3 channels on fixed, but non-permeabilized, cells followed by the intracellular staining of cortactin. Confocal images shown in Figure 1 revealed that the fluorescent signals of labeled membrane Kv1.3 channels (green) and cortactin (red) are highly overlapping which indicates that these proteins exist in close proximity to each other and predicts a possible interaction between them.

Cortactin/SH3/PDZ-binding site mutants of Kv1.3

Since confocal images suggested a possible association between Kv1.3 and cortactin, we compared the C-terminal end of Kv1.2 to that of Kv1.3 to determine whether the cortactin binding sequence identified in Kv1.2 was also present in Kv1.3 (Hattan *et al.*, 2002). A similar 19-amino-acid domain was identified in Kv1.3 (Fig. 2A). Moreover, SH3 (PxxP) and a PDZ binding (FTDV) motifs are also positioned on the C-terminal of Kv1.3 downstream of the putative cortactin binding site (Fig. 2B). Based on this analysis, we designed several mutants of Kv1.3 with altered C terminus. Sequential truncation of the C terminus resulted in constructs without any recognition sites (putative cortactin, SH3, PDZ: $\Delta 1$), only with putative cortactin-binding motif ($\Delta 2$; for sake of clarity from now on “putative cortactin-binding” is defined by simply “cortactin-binding”) and with cortactin- and SH3-binding domain ($\Delta 3$); and with mutation of few amino acids we obtained full length Kv1.3 channels without SH3-binding domain (Δ SH3) or PDZ-binding sequence (Δ PDZ) (Figure 2C). A C-terminal truncated mutant previously designed, Δ C, was also utilized (Szilágyi *et al.*, 2013). The effective neutralization of the SH3 domain in this Kv1.3 construct has been previously confirmed (Marks and Fadool,

2007). The inability of the Δ PDZ Kv1.3 mutant to bind PDZ proteins was established by immunoprecipitation (Supplemental Figure S1). Cells were co-transfected with myc-Dlg1 and either EGFP-tagged WT or Δ PDZ Kv1.3 clones. After immunoprecipitation of Dlg1, Kv1.3 was detected only in the cells transfected with wild-type (WT) Kv1.3. All these mutants can thus be used to obtain information on the site of Kv1.3 interaction with cortactin, and clarify whether other adaptor proteins (hDlg1, PSD95) are required for this linkage.

Electrophysiology of mutant channels

The deletion of the C-terminus of Kv1.x channels may lead to loss-of-function and inappropriate sorting of the proteins (Zhu *et al.*, 2003; Zhu *et al.*, 2007). Consequently, electrophysiological experiments were performed to verify the appropriate membrane targeting and assembly of each Kv1.3 mutant channel. Kv1.3 variants were transiently transfected into HEK-293 cells, and K⁺ currents were recorded in outside-out patches from cells expressing EGFP-tagged channels. Kinetic and equilibrium parameters of Kv1.3 channel's gating for Δ 1, Δ 2, Δ 3, Δ SH3 and Δ PDZ mutants and WT constructs were compared. The biophysical properties of Δ C was determined before (Szilágyi *et al.*, 2013). No differences were found between Δ C and WT Kv1.3 (Szilágyi *et al.*, 2013). As shown in Figure 3A, the current traces obtained upon a 2-s long depolarization from a patch expressing WT and Δ 1 plasmids are almost identical (not all mutants shown for clear visibility). To obtain time constant characteristics for inactivation the declining part of the current traces was fitted with one-exponential function (see Materials and Methods). Figure 3B demonstrates that none of the mutations introduced into Kv1.3 protein modifies the time constant of inactivation (τ_i) which was in ms for WT: 219 ± 22 (n=8), Δ 1: 233 ± 36 (n=5), Δ 2: 244 ± 33 (n=7), Δ 3: 249 ± 20 (n=8), Δ SH3: 257 ± 22 (n=8), Δ PDZ: 211 ± 34 (n=11) (p=0.831). Afterwards the steady-state parameters of the voltage-dependence of activation, which describes the opening probability of the channel at a certain membrane potential, were determined for all channel constructs: normalized whole-cell conductance was plotted against test potential and Boltzmann functions were fitted to the data points (only shown for WT and Δ 1 in Fig. 3C). We found that both half-maximal activation voltage ($V_{1/2}$) and slope factor (k) were not statistically different for any mutants of Kv1.3 (k was for WT: 12.2 ± 1.2 mV (n=5), Δ 1: 10.1 ± 1 mV (n=4) Δ 2: 11.3 ± 1.1 mV (n=6), Δ 3: 11.6 ± 0.4 mV (n=6) Δ SH3: 10.6 ± 0.4 mV (n=5) Δ PDZ: and 13.2 ± 1.2 mV (n=7) p=0.285; $V_{1/2}$ was for WT: -20.8 ± 3.5 mV (n=5), Δ 1: -22.0 ± 2.4 mV (n=4) Δ 2: -25.2 ± 1.6 mV (n=6), Δ 3: -18.7 ± 1.1 mV (n=6) Δ SH3: -20.9 ± 1.1 mV (n=5) Δ PDZ: and -19.6 ± 2.5 mV (n=7) p=0.32, Figure 3D). Consequently, the truncations and amino-acid replacements did not modify the biophysical characteristics of the channels.

Interaction of Kv1.3 with cortactin

We used Proximity Ligation Assay (PLA) to learn whether cortactin and Kv1.3 channels interact in HEK-293 cells and which portion of the channel protein is important for this association. This method enables detecting the interaction between proteins that reside at <40 nm distance through species-specific secondary antibodies each with unique short oligonucleotides and a polymerase that amplifies the circular DNA that is formed by hybridization when the two antibodies are in close proximity (Soderberg *et al.*, 2006). The GFP antibody, which recognizes the EGFP moiety at the N terminus of the Kv1.3 channels, was used along with the cortactin antibody. As shown in Fig 4A, HEK-293 cells expressing wild-type EGFP-Kv1.3 clone display positivity for PLA

signal: red dots. The same experiments were performed for cells transfected with $\Delta 1$, $\Delta 2$, $\Delta 3$, $\Delta SH3$ Kv1.3 mutants. Confocal images were analyzed for number of dots and the results are summarized in Fig. 4B. The number of dots/cell in WT Kv1.3 is significantly different than in all the Kv1.3 mutants ($p < 0.001$). Furthermore, the PLA signal in the $\Delta 3$ mutant is significantly higher than that in $\Delta 1$, $\Delta 2$ and $\Delta SH3$ mutants ($p < 0.001$). These findings suggest that cortactin binds Kv1.3 in intact cells and that the association between these proteins occurs through the SH3-binding domain. Further PLA experiments confirmed the close proximity and interaction of cortactin with actin thus suggesting a role for cortactin in linking Kv1.3 to the actin cytoskeleton (Fig. 4C) (Daly, 2004). We then tested whether the lateral membrane motility of Kv1.3 depends on an active process that is mediated by actin and whether cortactin guarantees the association between Kv1.3 and actin.

Lateral mobility of Kv1.3 channel constructs

The lateral membrane motility of Kv1.3 and its dependence on the actin cytoskeleton and cortactin were established in (Fluorescence Recovery after Photobleaching) FRAP experiments. The recovery of fluorescence in the plasma membrane after photobleaching occurred by lateral membrane diffusion for all transfected Kv1.3 channels as can be seen by the time series of Kv1.3 fluorescent recovery depicted in Figure 5A and, for WT Kv1.3, in a supplemental movie (Supplemental Movie 1). Analysis of FRAP recovery curves yielded an estimate of the mobile fraction (M_f) of Kv1.3 channels (Fig. 5A and B). Alterations of Kv1.3 membrane mobility by actin polymerization were determined to establish the role that actin has on the channel motility. Where indicated jasplakinolide, which is a cyclic peptide of *Jaspis johnstoni* (a marine sponge), was applied for 50 min before FRAP experiments to induce actin polymerization and stabilization of the filaments (Bubb *et al.*, 1994; Bubb *et al.*, 2000). The addition of jasplakinolide caused a significant reduction in M_f in the WT, $\Delta 3$, and ΔPDZ mutants of 40-50% compared to cells that were not pre-treated with jasplakinolide, but jasplakinolide did not affect the M_f of $\Delta 1$, $\Delta 2$, and $\Delta SH3$ mutants (Fig. 5). The average M_f of all channel mutants without jasplakinolide pre-treatment was 0.71 ± 0.01 ($n=41$, Fig. 5B). The average M_f of WT, $\Delta 3$, and ΔPDZ channels treated with jasplakinolide was 0.43 ± 0.01 ($n=18$), while the average M_f of $\Delta 1$, $\Delta 2$, and $\Delta SH3$ channels treated with jasplakinolide was 0.63 ± 0.01 ($n=15$). These outcomes support the importance of the SH3-binding domain in the functional interaction between the channel and actin cytoskeleton.

Role of cortactin in Kv1.3 mobility

FRAP experiments with mutant channels confirmed that cortactin and actin have a role in Kv1.3 channel immobilization. Hence, we used another approach to test the role of cortactin: a HEK-293 cell line with depleted cortactin level was established using lentiviral shRNA transduction. Figure 6A shows that cortactin expression was significantly reduced in cortactin-shRNA virus particle infected cells (control: non-target/scramble shRNA transduced cells). As a next step we expressed EGFP-tagged wild-type Kv1.3 channels in these cell lines, and subjected them to FRAP experiments with or without jasplakinolide treatment (Fig. 6B). The M_f of Kv1.3 channels in cortactin knock-down cells was the same regardless the pre-incubation with jasplakinolide or not (M_f : 0.61 ± 0.03 for control ($n=5$), and 0.50 ± 0.08 for jasplakinolide ($n=5$), $p=0.43$). On the contrary, the mobility of wild-type channels significantly dropped in control shRNA transduced

cells when actin stabilization was provoked by jasplakinolide (M_f : 0.66 ± 0.04 for control ($n=4$); and 0.41 ± 0.09 for jasplakinolide ($n=4$), $p=0.033$). These studies further confirm the role of cortactin in the F-actin mediated lateral motility of Kv1.3.

Interaction of Kv1.3 and HS1 in T lymphocytes

The studies reported so far demonstrated that an association exists between recombinant Kv1.3 channels and cortactin in HEK-293 cells. Further immunohistochemistry experiments in primary T cells showed that native Kv1.3 channels and HS1 (the cortactin analog expressed in T cells) co-localize at the IS (Fig. 7A). Primary human T cells were activated with beads coated with anti-CD3 and anti-CD28 antibodies (CD3/CD28 beads). These beads mimic APCs: they bind to the T cells, induce the formation of the IS and activate them (Nicolaou *et al.*, 2007). Cells coupled with CD3/CD28 beads were stained for endogenous Kv1.3 (green) and HS1 (red). The merge image in Figure 7A shows co-localization of these two proteins at the bead/T cell contact point (the IS). The actual interaction between Kv1.3 and HS1 at the IS was established by PLA experiments in Jurkat T cells stably expressing GFP-tagged WT Kv1.3 channels (Fig. 7B-C). PLA positive signal was present at the IS where Kv1.3 accumulate (Supplemental Fig. 2). On the contrary, when PLA was performed on cells that expressed truncated ΔC Kv1.3 channels (see also Fig. 2C), although these channels are recruited at the IS, they do not interact with HS1 as indicated by the significant drop in the PLA signal (Fig. 7B-C). Similarly, WT Kv1.3 channels do not associate with HS1 in resting T cells, which were not exposed to CD3/CD28 beads (no IS). These data indicate that Kv1.3-HS1 interaction occurs only upon activation of T cells and is strictly happening at the IS. Furthermore they emphasize that HS1 in T lymphocytes, like cortactin in HEK-293 cells, interact with Kv1.3 via the carboxyl terminal of the channel.

DISCUSSION

As described by various groups, cortactin can bind to ion channels; however, the site of interaction is still unresolved. An extensive study performed by the workgroup of Morielli described the 19-amino acid span on the C-terminus of the Kv1.2 channel as an essential element in the channel's coupling to cortactin (Williams *et al.*, 2007; Cheng *et al.*, 2011). Furthermore, this group also described that fusion of the SH3 binding domain with the truncated Kv1.2, which does not have the cortactin binding site, can partially restore the coupling of cortactin to the channel (Hattan *et al.*, 2002; Williams *et al.*, 2007). Surprisingly, the phosphorylation of tyrosine residues upstream of the cortactin binding domain of Kv1.2 abolished the interaction between the channel and cortactin (Hattan *et al.*, 2002; Williams *et al.*, 2007). Others showed that cortactin binds directly to the SH3-binding domains of the C terminal region of ENaC (epithelial sodium channel) and BKCa (large conductance Ca^{2+} -activated K) channels, without any adaptor proteins (Tian *et al.*, 2006; Ilatovskaya *et al.*, 2011). Here we demonstrated by means of the PLA that in an intact cell, the interaction between cortactin and Kv1.3 channels exclusively occurs through the SH3 domain, and the other potential binding sequences of the Kv1.3 have hardly any influence on this coupling. These data indicate that other cortactin-binding sites existing on the Kv1.3 protein are unavailable in an intact cell setting where they may be masked by post-translational modifications and/or the presence of other proteins that compete for those sites. Experiments with the ΔPDZ mutant showed that disruption of the PDZ-binding domain did not

modify cortactin-channel binding, which confirms the direct coupling between Kv1.3 and cortactin. This is in agreement to what reported in the literature for other channels (Tian *et al.*, 2006; Ilatovskaya *et al.*, 2011). Further PLA experiments verified that the Kv1.3-HS1 interaction in Jurkat T cells occurs via the C-terminus of the channel. Nevertheless, this coupling is not constitutive and triggered by TCR activation and intracellular mediators not yet known as the PLA positivity was only seen in the IS-engaged but not standalone T cells (Fig. 7). Overall, these results point to the existence of a physical association between cortactin (and HS1) and Kv1.3, and its possible role in cytoskeleton-regulated functions.

The functional studies reported herein discovered a role for actin and cortactin in Kv1.3 membrane motility. The FRAP studies revealed that actin polymerization/remodeling induced by jasplakinolide can lead to a significant decrease in M_f of Kv1.3 channels, which were described to ramble more-or-less freely in the plasma membrane (O'Connell and Tamkun, 2005). Herein we provide evidence for a role of the actin cytoskeleton in locking Kv1.3 and limiting its diffusion in the plasma membrane. Binding of PDZ proteins to Kv channels was shown to induce clustering of Kv1.3, Kv1.4, and Kv1.5 channels into cell surface domains and reduce Kv1.5 cell membrane mobility (Imamura *et al.*, 2002; Marks and Fadool, 2007). In our studies, PDZ-domain adaptor proteins such as hDlg and PSD-95 were excluded as regulators of Kv1.3 membrane motility (the M_f of the Δ PDZ mutant before actin polymerization is equivalent to that of WT channels) and as linkers of the cortical cytoskeleton and Kv1.3. Mutating the PDZ-binding domain (Δ PDZ) we could observe the same immobilization of the channels upon jasplakinolide treatment like it was observed in WT Kv1.3. Both $\Delta 1$ and $\Delta 2$ mutants instead showed no significant “arrest” by the induction of actin polymerization (Fig. 5), indicating that the putative cortactin-binding site is insufficient to provide a functional attachment of Kv1.3 to the cytoskeleton. Upon “re-addition” of SH3-binding site ($\Delta 3$) the drop in M_f after actin-polymerization was comparable to that of wild-type channels. Conversely, mutation of the SH3-binding motif (Δ SH3) cancelled the channel’s immobilization by jasplakinolide. Overall, these data support a model in which the interaction between cortactin and Kv1.3 has functional implications only when actin-remodeling is induced. When no actin-polymerization occurs, the channels presumably diffuse freely along the plane of the membrane but upon actin-polymerization the channel-cortactin complex becomes trapped by the F-actin network. Consequently, the SH3-binding motif provides the interface for cortactin-Kv1.3 coupling as reported for ENaC and BKCa, and confirmed by the PLA results.

Cortactin has also been reported to regulate the surface expression of ion channels (Hattan *et al.*, 2002; Williams *et al.*, 2007; Cheng *et al.*, 2011; Herrmann *et al.*, 2012). By patch-clamping we found that all EGFP-tagged Kv1.3 mutant plasmids were expressed in HEK-293 cells and could form conducting tetrameric channels. It has been described recently that two glutamic acids (E) at position 483 and 484 of Kv1.3 carboxyl terminus are the part of the cell membrane sorting sequence and aids forward trafficking (Martínez-Mármol *et al.*, 2013). Here we observed that their removal in the $\Delta 1$ construct did not influence the detection of EGFP signal in the plasma membrane. Nevertheless, we cannot exclude that $\Delta 1$ truncation leads to a lower expression level in the whole-cell configuration (here we used outside-out patches), and that assembly with endogenous Kv1.3 subunits in HEK-293 steered the heteromeric channels to the plasma membrane. We must note that for our ΔC mutant we did not obtain different expression level in Jurkat T cells as compared to the wild-type Kv1.3 (Szilagyi *et al.*, 2013). Hence, we extrapolate the same to be true for all Kv1.3 constructs tested here. As the channels

were overexpressed in HEK-293 cells a possible reduction in the mutant channel's targeting to the membrane had no impact on the measurement of Kv1.3 diffusion as indicated by the similar values of baseline M_f (before jasplakinolide addition).

Finally, knock-down of cortactin clearly demonstrated that assemblage of F-actin with Kv1.3 channels is mediated by cortactin upon jasplakinolide stimulation. Wild-type Kv1.3 channels expressed in cortactin-silenced cells did not show immobilization by jasplakinolide treatment unlike channels transfected into scramble shRNA-treated cell line (Fig. 6B). Due to the elimination of the linker element, Kv1.3 channels are not affixed to the cytoskeleton and, upon actin remodeling, can freely move in the plasma membrane. Hence, cortactin has a pivotal role in the anchoring of Kv1.3 channels.

In this study we could show that the pore-forming alpha subunit of another potassium ion channel is coupled to the cortical actin network, which stabilizes it upon F-actin nucleation. Since Kv1.3 channels are part of molecular machinery required for activation of T cells, our results may provide new insights into the mechanisms that control Kv1.3 membrane localization in the IS which is of great importance in T cell function. The PLA experiments in T cells showed that the lack of a HS1-binding site does not preclude the channel from entering the IS, suggesting that HS1 may not affect Kv1.3 diffusion into the IS. Therefore, it is possible that HS1 may alter the time Kv1.3 resides in the IS or its association with signaling molecules also residing at the IS that ultimately control its activity (Nicolaou *et al.*, 2010; Kuras *et al.*, 2012). However, these hypotheses should be tested to understand functional significance of HS1-Kv1.3 interaction in T cells. Overall, the results presented herein raise the possibility that the association between HS1 and Kv1.3 channels may shape the outcome of the signaling pathways during T cell activation.

MATERIALS AND METHODS

Kv1.3 channel constructs

Plasmids (pEGFP-C1 backbone, Clontech) containing EGFP tagged wild-type (WT) and mutant Kv1.3 channels were generated for expression in human embryonic kidney (HEK-293) cells. EGFP attachment to the N-terminus of Kv1.3 constructs was performed as previously described (Nicolaou *et al.*, 2010). C-terminal Kv1.3 mutants were generated by either amino acid sequence truncations or specific amino acid mutagenesis. Truncated C-terminal Kv1.3 mutants were created by insertion of a premature stop codon into the Kv1.3 DNA sequence prior to the specified truncation site. Truncation sites were specified just prior to the presumed cortactin binding site at amino acid 466 ($\Delta 1$ mutant), after the presumed cortactin binding site at amino acid 487 ($\Delta 2$ mutant), and after an SH3 binding motif (-P-x-x-P-) at amino acid 496 ($\Delta 3$). Presumed cortactin binding site of Kv1.3 was determined from analogous amino acid sequence in Kv1.2 (Hattan *et al.*, 2002). A C-terminal mutant with altered SH3 binding motif (Δ SH3) was generated by changing proline residues at amino acids 493 and 496 to glycines, and a C-terminal mutant with altered PDZ binding domain (Δ PDZ) was generated by changing the amino acid sequence FTDV at the end of the C-terminus to WSGG. Plasmid for the Δ SH3 mutant was a gift from Dr. Fadool (Florida State University) and has been previously described (Marks and Fadool, 2007). A schema of Kv1.3 wild type and C-terminal mutants can be found in Figure 2. We generated a construct for rat Kv1.3 containing a FLAG tag between D222 and V223 in the extracellular loop between S1 and S2 transmembrane domains. Briefly, a DNA fragment

containing the nucleotide sequence corresponding to a FLAG tag (YKDDDDK) was generated by two-step overlapped PCR. The generated fragment was replaced with the corresponding portion of Kv1.3 cDNA using *SphI* and *PstI* sites. The sequence of the PCR amplified portion was verified by DNA sequencing.

Cell culture and transfection

HEK-293 cells were cultured in DMEM media (Fisher Scientific) supplemented with 10% fetal bovine serum, 1 mM Na-pyruvate, 200 unit penicillin/streptomycin (HEK-293 medium). HEK-293 cells stably expressing FLAG tagged Kv1.3 channels or host plasmid (pcDNA3.1) were also grown in HEK-293 medium containing 1 mg/ml G418 (Sigma-Aldrich). Transfections of DNA plasmids were done using Lipofectamine 2000TM (Life Technologies) according to the manufacturer's protocol. For cortactin knockdown experiments HEK-293 cells were transduced with lentiviral-based shRNA virus particles produced at the Lenti-shRNA Library Core, Cincinnati Children's Hospital (www.cincinnatichildrens.org/research/cores/lenti/). The protocol for viral infection and cell culturing (puromycin selection) is available at www.cincinnatichildrens.org/research/cores/lenti/background-protocol/. Briefly, HEK-293 cells were plated 24 hours prior to lentiviral transduction in DMEM medium. Next day the medium was replaced with fresh DMEM medium containing 10 µg/ml polybrene (Sigma-Aldrich) and lentiviral supernatant which contained virus particles with cortactin or negative control shRNAs (Mission shRNA, Sigma-Aldrich). Non-target shRNA containing virus particles were used as negative control. Knockdown cells were selected with 1-2 µg/ml puromycin (Sigma-Aldrich). The efficiency of knock-down was monitored with Western blot technique.

Primary T and Jurkat cells

Human T cells were isolated from the blood of healthy consenting donors and discarded blood units from Hoxworth Blood Center (UC, Cincinnati) using RosetteSepTM Human Total Lymphocyte Enrichment Cocktail (StemCell Technologies). The protocol was approved by University of Cincinnati IRB. T cells were maintained in RPMI-1640 medium supplemented with 10% human serum, 200 U/ml penicillin, 200 µg/ml streptomycin and 10 mM HEPES (T cell medium). Jurkat E6-1 cells were maintained in RPMI-1640 medium with 10% human serum, 200 U/ml penicillin, 200 µg/ml streptomycin 10 mM HEPES and passed every other day. Stable-transfected WT and ΔC Kv1.3 Jurkat T cells were described previously (Szilágyi *et al.*, 2013).

Electrophysiology

HEK-293 cells transfected with various Kv1.3 channel constructs were washed with standard bath solution (composition was in mM: 145 NaCl, 5 KCl, 1 MgCl₂, 2.5 CaCl₂, 5.5 glucose, 10 HEPES), and plated onto poly-L-lysine coated glass coverslips. Kv1.3 currents were recorded in outside-out configuration using Axopatch 200B amplifier (Axon Instruments, Foster City, CA, USA) as previously described (Szigligeti *et al.*, 2006). The pipette solution contained (in mM): 140 KF, 11 K₂EGTA, 1 CaCl₂, 2 MgCl₂, and 10 HEPES (pH 7.20, ~295 mOsm). P/5 protocol for

online leaks subtraction was applied to minimize capacitance and leak errors during the determination of the activation kinetics.

The inactivation kinetics of each construct was determined upon fitting a single exponential function ($I(t) = I_0 \times \exp(-t/\tau_i) + C$, I_0 : amplitude of current, τ_i : inactivation time constant, C : steady-state value of whole-cell current at the end of the pulse) to the decaying part of the traces evoked by 2-s-long depolarization to +40 mV from a holding potential (HP) of -120 mV.

The voltage-dependence of steady-state activation was determined as detailed below. The outside-out patches were clamped at -120 mV HP and depolarizing test potentials from -70 up to +50 mV were in 10 mV steps delivered every 30 s. Peak conductance ($G(V)$) at each test potential was calculated from the peak current (I_p) at test potential (V) and the K^+ reversal potential ($E_r = -85$ mV) with the equation $G(V) = I_p / (V - E_r)$. The $G(V)$ values were normalized for the maximum conductance and plotted against the test potential. Boltzmann-function was fitted to the data points: $G_N = 1 / (1 + \exp[-(V - V_{1/2})/k])$, where G_N is the normalized conductance, V is the test potential, $V_{1/2}$ is the midpoint and k is the slope of the function.

Immunocytochemistry

HEK-293 cells stably expressing FLAG-Kv1.3 encoding plasmid or empty vector (pcDNA3.1, Life Technologies) were plated onto poly-L-lysine coverslips and incubated for 3-4 hrs (37 °C, humidified, 5 % CO_2). Then cells were fixed with 1% formaldehyde, and labeled with rabbit anti-FLAG antibody (10 μ g/ml, Sigma-Aldrich Ltd.) overnight at 4 °C. Afterwards cells were permeabilized with 0.2% Triton-X 100 for 20 min at room temperature, and mouse anti-cortactin antibody (1:50 dilution; Santa-Cruz) was added overnight at 4 °C. Secondary antibodies (donkey anti-rabbit with Alexa488, goat anti-mouse with Alexa647, Life Technologies) were added to the cells for 1 hour at room temperature. Finally coverslips were mounted onto slides with Fluoromount G (eBioScience). Zeiss LSM 510 META microscope was used to take confocal images of the cells (63 \times oil immersion lens, NA 1.4). The He-Ne laser was selected to excite fluorophore Alexa647 (line 633 nm) and Argon laser (line 488 nm) to visualize Alexa488. The thickness of the slices and z-stacks were set to 1 μ m.

Immunological synapse were formed between either resting T lymphocytes or Jurkat T cells and anti-CD3/anti-CD28 antibody (CD3/CD28) coated polystyrene beads (Life Technologies) as detailed earlier (Nicolaou *et al.*, 2007). Cell-bead conjugates were fixed 5 and 30 min after synapse formation and labelled with rabbit anti-Kv1.3 antibody (Alomone, Israel) at 4 °C overnight. Then the cells were permeabilized as described for HEK-293 cells and goat anti-HS1 antibody (R&D Systems, USA) was added. The secondary antibodies (goat anti rabbit IgG A488, donkey anti goat A647, Life Technologies) were incubated for 1 hour at room temperature. Afterwards coverslips were mounted onto slides with Fluoromount G. The confocal snapshots were taken as described above.

Western blotting

For shRNA experiments, transfected HEK-293 cells were lysed using Pierce[®] IP Lysis Buffer along with HALT Protease Inhibitor[™] cocktail (ThermoFisher Scientific) as previously described (Chimote *et al.*, 2012). The protein content of the lysates was measured using the BCA Protein Assay (ThermoFisher Scientific). Cell lysates were mixed with 3X SDS sample buffer

(New England Biolabs) and 20 µg of protein was loaded on to each lane of a 4-12% TRIS-glycine gel (Life Technologies) in a X Cell SureLock™ Gel System (Life Technologies). The protein bands were transferred to a PVDF membrane (Life Technologies) in a X Cell II Blot Module (Life Technologies). The membrane was blocked with Odyssey Blocking buffer (Licor Biosciences) at room temperature for 1 h and subsequently incubated overnight at 4 °C with a polyclonal rabbit antibody against cortactin (SantaCruz Biotechnology Inc) along with a mouse monoclonal antibody against β -actin (Alpha Diagnostic International). The blot was thoroughly washed with PBS-T and incubated with Alexa Fluor 680 anti-rabbit and IRDye 800CW anti-mouse secondary antibodies for 60 min at room temperature (Life Technologies). The blots were then visualized with the LI-COR Odyssey® infrared scanner at 169µm resolution.

Proximity ligation assay

Proximity ligation assay (PLA) experiments were performed using Duolink® In Situ PLA® Kit (Sigma-Aldrich) with Detection Reagents Red as suggested by the manufacturer's protocol. HEK-293 cells were transfected with EGFP-tagged Kv1.3 constructs, then plated onto poly-L-lysine coated coverslips. Primary antibodies were mouse anti-GFP (1:200, Miltenyi Biotec) and rabbit anti-cortactin (1:200, Santa-Cruz Biotechnology Inc.). Jurkat cells stably expressing GFP-WT or Δ C Kv1.3 channels were incubated with CD3/CD28 beads for 30 min, plated on poly-L-lysine coated coverslips. Cells incubated without the beads were used as controls (resting, no IS, T cells). Cells were fixed permeabilized and then incubated with mouse anti-GFP (1:200, Miltenyi Biotec) and goat anti-HS1 (1:200, R&D systems). Confocal images were taken with a Zeiss LSM 710 microscope with 63× water immersion lens (pinhole was set to 1 Airy unit). Individual interacting molecule pairs are detected as bright fluorescent spots. Evaluation of PLA snapshots was done by the Duolink Image Tool software (demo version) which allows quantitating the PLA signal.

Fluorescence recovery after photobleaching (FRAP)

Transfected HEK-293 cells were plated onto collagen and poly-L-lysine coated glass coverslips and incubated in DMEM without phenol red at 37 °C for at least 1 hour before performing FRAP experiments. Cells were also bathed in DMEM without phenol red during FRAP measurements. A subset of cell coverslips was also bathed in a solution containing the actin polymerizing agent jasplakinolide (Calbiochem) (2 µM; DMSO 1:1000 dilution in control cells) for 50 minutes at 37 °C prior to FRAP measurements. FRAP experiments were performed on a Zeiss LSM 510 Meta confocal microscope with a 40× water immersion objective (NA 1.2) at room temperature. Pinhole size was set between 0.8-0.86 µm (slice thickness was approximately 1 µm). During the measurements EGFP-tagged Kv1.3 channels were excited with a 488 nm Argon laser that was passed through an EGFP-filter of 505-535 nm at 1% power for pre- and post-bleach measurements. Photobleaching was confined to a region of interest (ROI) only along the cell membrane and was performed with the Argon laser (488 nm) at 100% power for 100 bleach iterations over this ROI. Confocal images during FRAP experiments were acquired every 15 seconds at a resolution of 512x512 and 3x zoom for a total of 60 scans. The background fluorescence was subtracted from the average fluorescent intensity over the photobleached ROI

from each image and then normalized to the pre-bleach intensity. These normalized values were used for the final analysis. The mobile fraction (M_f) was determined using

$$M_f = \frac{F_\infty - F_0}{F_i - F_0} \quad (1)$$

where F_∞ is the fluorescence at the end of the FRAP experiments, F_0 is the fluorescence intensity immediately post-bleach, and F_i is the fluorescence pre-bleach.

Statistical analysis

Data are expressed as the mean \pm standard error. Means were compared using Student's t-test, One-Way ANOVA and One-Way ANOVA on Ranks. P-values <0.05 were considered statistically significant. Statistical analyses were performed using SPSS version 21.0 (SPSS Inc.).

ACKNOWLEDGMENTS

Technical assistance of Lisa Neumeier and Charles Ebersbacher is really appreciated. This project was funded in part by AHA Grant-in-Aid #0855457D and NIH R01CA095286. O.S. was supported by the European Union and the State of Hungary, co-financed by the European Social Fund in the framework of TÁMOP 4.2.4. A/2-11-1-2012-0001 'National Excellence Program'. The authors confirm that there are no known conflicts of interest associated with this publication and there has been no significant financial support for this work that could have influenced its outcome.

REFERENCES

- Babich, A., Li, S., O'Connor, R.S., Milone, M.C., Freedman, B.D., and Burkhardt, J.K. (2012). F-actin polymerization and retrograde flow drive sustained PLC γ 1 signaling during T cell activation. *The Journal of cell biology* 197, 775-787.
- Bubb, M.R., Senderowicz, A.M., Sausville, E.A., Duncan, K.L., and Korn, E.D. (1994). Jasplakinolide, a cytotoxic natural product, induces actin polymerization and competitively inhibits the binding of phalloidin to F-actin. *J Biol Chem* 269, 14869-14871.
- Bubb, M.R., Spector, I., Beyer, B.B., and Fosen, K.M. (2000). Effects of jasplakinolide on the kinetics of actin polymerization. An explanation for certain in vivo observations. *J Biol Chem* 275, 5163-5170.
- Cahalan, M.D., and Chandy, K.G. (2009). The functional network of ion channels in T lymphocytes. *Immunological reviews* 231, 59-87.
- Carrizosa, E., Gomez, T.S., Labno, C.M., Klos Dehring, D.A., Liu, X., Freedman, B.D., Billadeau, D.D., and Burkhardt, J.K. (2009). Hematopoietic Lineage Cell-Specific Protein 1 Is Recruited to the

Immunological Synapse by IL-2-Inducible T Cell Kinase and Regulates Phospholipase C γ 1 Microcluster Dynamics during T Cell Spreading. *The Journal of Immunology* 183, 7352-7361.

Cheng, L., Yung, A., Covarrubias, M., and Radice, G.L. (2011). Cortactin Is Required for N-cadherin Regulation of Kv1.5 Channel Function. *Journal of Biological Chemistry* 286, 20478-20489.

Chimote, A.A., Kuras, Z., and Conforti, L. (2012). Disruption of kv1.3 channel forward vesicular trafficking by hypoxia in human T lymphocytes. *J Biol Chem* 287, 2055-2067.

Daly, R.J. (2004). Cortactin signalling and dynamic actin networks. *Biochem. J.* 382, 13-25.

Davis, S.J., and van der Merwe, P.A. (2006). The kinetic-segregation model: TCR triggering and beyond. *Nature immunology* 7, 803-809.

Doczi, M.A., Damon, D.H., and Morielli, A.D. (2011). A C-terminal PDZ binding domain modulates the function and localization of Kv1.3 channels. *Experimental Cell Research* 317, 2333-2341.

Douglass, A.D., and Vale, R.D. (2005). Single-molecule microscopy reveals plasma membrane microdomains created by protein-protein networks that exclude or trap signaling molecules in T cells. *Cell* 121, 937-950.

Dushek, O., Mueller, S., Soubies, S., Depoil, D., Caramalho, I., Coombs, D., and Valitutti, S. (2008). Effects of Intracellular Calcium and Actin Cytoskeleton on TCR Mobility Measured by Fluorescence Recovery. *PloS one* 3, e3913.

Dustin, M.L. (2007). Cell adhesion molecules and actin cytoskeleton at immune synapses and kinapses. *Current Opinion in Cell Biology* 19, 529-533.

Favier, B., Burroughs, N.J., Wedderburn, L., and Valitutti, S. (2001). TCR dynamics on the surface of living T cells. *International immunology* 13, 1525-1532.

Gomez, T.S., McCarney, S.D., Carrizosa, E., Labno, C.M., Comiskey, E.O., Nolz, J.C., Zhu, P., Freedman, B.D., Clark, M.R., Rawlings, D.J., Billadeau, D.D., and Burkhardt, J.K. (2006). HS1 functions as an essential actin-regulatory adaptor protein at the immune synapse. *Immunity* 24, 741-752.

Hajdu, P., Chimote, A.A., Thompson, T.H., Koo, Y., Yun, Y., and Conforti, L. (2013). Functionalized liposomes loaded with siRNAs targeting ion channels in effector memory T cells as a potential therapy for autoimmunity. *Biomaterials* 34, 10249-10257.

Hattan, D., Nesti, E., Cachero, T.G., and Morielli, A.D. (2002). Tyrosine phosphorylation of Kv1.2 modulates its interaction with the actin-binding protein cortactin. *J Biol Chem* 277, 38596-38606.

Herrmann, S., Ninkovic, M., Kohl, T., Lörinczi, É., and Pardo, L.A. (2012). Cortactin Controls Surface Expression of the Voltage-gated Potassium Channel KV10.1. *Journal of Biological Chemistry* 287, 44151-44163.

Hu, L., Wang, T., Gocke, A.R., Nath, A., Zhang, H., Margolick, J.B., Whartenby, K.A., and Calabresi, P.A. (2013). Blockade of Kv1.3 Potassium Channels Inhibits Differentiation and Granzyme B Secretion of Human CD8+ T Effector Memory Lymphocytes. *PloS one* 8, e54267.

Ilatovskaya, D.V., Pavlov, T.S., Levchenko, V., Negulyaev, Y.A., and Staruschenko, A. (2011). Cortical actin binding protein cortactin mediates ENaC activity via Arp2/3 complex. *The FASEB Journal* 25, 2688-2699.

Imamura, F., Maeda, S., Doi, T., and Fujiyoshi, Y. (2002). Ligand Binding of the Second PDZ Domain Regulates Clustering of PSD-95 with the Kv1.4 Potassium Channel. *Journal of Biological Chemistry* 277, 3640-3646.

Kummerow, C., Junker, C., Kruse, K., Rieger, H., Quintana, A., and Hoth, M. (2009). The immunological synapse controls local and global calcium signals in T lymphocytes. *Immunological reviews* 231, 132-147.

Kuras, Z., Yun, Y.H., Chimote, A.A., Neumeier, L., and Conforti, L. (2012). KCa3.1 and TRPM7 channels at the uropod regulate migration of activated human T cells. *PloS one* 7, e43859.

Marks, D.R., and Fadool, D.A. (2007). Post-synaptic density perturbs insulin-induced Kv1.3 channel modulation via a clustering mechanism involving the SH3 domain. *Journal of neurochemistry* 103, 1608-1627.

Martínez-Mármol, R., Pérez-Verdaguer, M., Roig, S.R., Vallejo-Gracia, A., Gotsi, P., Serrano-Albarrás, A., Bahamonde, M.I., Ferrer-Montiel, A., Fernández-Ballester, G., Comes, N., and Felipe, A. (2013). A

non-canonical di-acidic signal at the C-terminus of Kv1.3 determines anterograde trafficking and surface expression. *Journal of Cell Science* 126, 5681-5691.

Mossman, K.D., Campi, G., Groves, J.T., and Dustin, M.L. (2005). Altered TCR signaling from geometrically repatterned immunological synapses. *Science* 310, 1191-1193.

Nicolaou, S.A., Neumeier, L., Steckly, A., Kucher, V., Takimoto, K., and Conforti, L. (2009). Localization of Kv1.3 channels in the immunological synapse modulates the calcium response to antigen stimulation in T lymphocytes. *J Immunol* 183, 6296-6302.

Nicolaou, S.A., Neumeier, L., Takimoto, K., Lee, S.M., Duncan, H.J., Kant, S.K., Mongey, A.B., Filipovich, A.H., and Conforti, L. (2010). Differential calcium signaling and Kv1.3 trafficking to the immunological synapse in systemic lupus erythematosus. *Cell calcium* 47, 19-28.

Nicolaou, S.A., Szigligeti, P., Neumeier, L., Lee, S.M., Duncan, H.J., Kant, S.K., Mongey, A.B., Filipovich, A.H., and Conforti, L. (2007). Altered dynamics of Kv1.3 channel compartmentalization in the immunological synapse in systemic lupus erythematosus. *J Immunol* 179, 346-356.

O'Connell, K.M., and Tamkun, M.M. (2005). Targeting of voltage-gated potassium channel isoforms to distinct cell surface microdomains. *J Cell Sci* 118, 2155-2166.

Shin, H., Hsueh, Y.-P., Yang, F.-C., Kim, E., and Sheng, M. (2000). An Intramolecular Interaction between Src Homology 3 Domain and Guanylate Kinase-Like Domain Required for Channel Clustering by Postsynaptic Density-95/SAP90. *The Journal of Neuroscience* 20, 3580-3587.

Soderberg, O., Gullberg, M., Jarvius, M., Ridderstrale, K., Leuchowius, K.-J., Jarvius, J., Wester, K., Hydbring, P., Bahram, F., Larsson, L.-G., and Landegren, U. (2006). Direct observation of individual endogenous protein complexes in situ by proximity ligation. *Nat Meth* 3, 995-1000.

Szigligeti, P., Neumeier, L., Duke, E., Chougnat, C., Takimoto, K., Lee, S.M., Filipovich, A.H., and Conforti, L. (2006). Signalling during hypoxia in human T lymphocytes--critical role of the src protein tyrosine kinase p56Lck in the O₂ sensitivity of Kv1.3 channels. *The Journal of physiology* 573, 357-370.

Szilágyi, O., Boratko, A., Panyi, G., and Hajdu, P. (2013). The role of PSD-95 in the rearrangement of Kv1.3 channels to the immunological synapse. *Pflügers Archiv : European journal of physiology* 465, 1341-1353.

Szilágyi, O., Boratkó, A., Panyi, G., and Hajdu, P. (2013). The role of PSD-95 in the rearrangement of Kv1.3 channels to the immunological synapse. *Pflügers Arch - Eur J Physiol* 465, 1341-1353.

Tian, L., Chen, L., McClafferty, H., Sailer, C.A., Ruth, P., Knaus, H.G., and Shipston, M.J. (2006). A noncanonical SH3 domain binding motif links BK channels to the actin cytoskeleton via the SH3 adapter cortactin. *FASEB J* 20, 2588-2590.

Williams, M.R., Markey, J.C., Doczi, M.A., and Morielli, A.D. (2007). An essential role for cortactin in the modulation of the potassium channel Kv1.2. *Proc Natl Acad Sci U S A* 104, 17412-17417.

Wulff, H., Calabresi, P.A., Allie, R., Yun, S., Pennington, M., Beeton, C., and Chandy, K.G. (2003). The voltage-gated Kv1.3 K(+) channel in effector memory T cells as new target for MS. *The Journal of clinical investigation* 111, 1703-1713.

Xavier, R., Rabizadeh, S., Ishiguro, K., Andre, N., Ortiz, J.B., Wachtel, H., Morris, D.G., Lopez-Illasaca, M., Shaw, A.C., Swat, W., and Seed, B. (2004). Discs large (Dlg1) complexes in lymphocyte activation. *The Journal of cell biology* 166, 173-178.

Zhu, J., Gomez, B., Watanabe, I., and Thornhill, W.B. (2007). Kv1 potassium channel C-terminus constant HRETE region: arginine substitution affects surface protein level and conductance level of subfamily members differentially. *Mol Membr Biol* 24, 194-205.

Zhu, J., Watanabe, I., Gomez, B., and Thornhill, W.B. (2003). Trafficking of Kv1.4 potassium channels: interdependence of a pore region determinant and a cytoplasmic C-terminal VXXSL determinant in regulating cell-surface trafficking. *Biochem J* 375, 761-768.

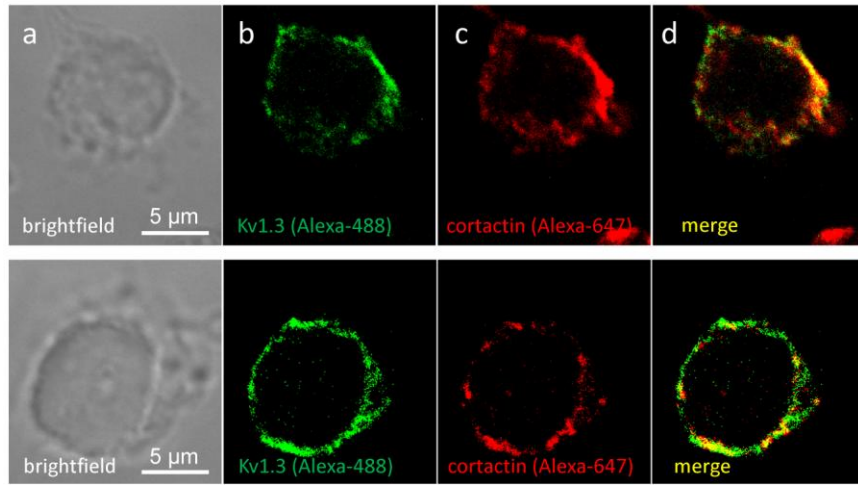
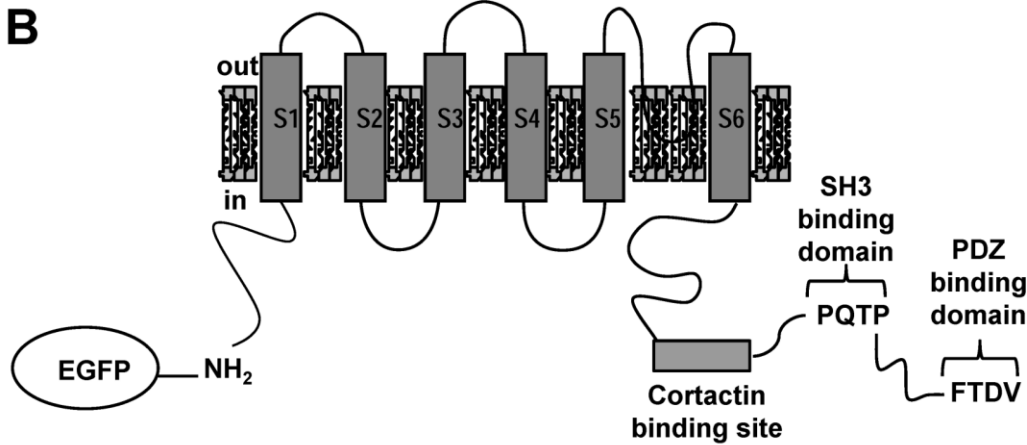


Figure 1. Kv1.3 channels co-localize with cortactin. Confocal images of 1 μm thickness of two representative FLAG-Kv1.3 expressing HEK-293 cells labeled with FLAG and cortactin antibodies. Panels show: *a*: brightfield image of the cell, *b*: Kv1.3 (green), *c*: cortactin (red), *d*: overlay of red and green channels. Note that overlapping of the red and the green signal turns yellow, which indicates co-localization. Panel is representative of 3 independent experiments.

A

Kv1.3-465 R**KARSNSTLSKSEYMVIEE**GG (485)
 Kv1.2-445 K**KRSASTISKSDYMEIQE**GV (465)
 :*:*** **:*****:** *:**

B**C**

WT: NFN~~Y~~F~~Y~~HRETEGEEQSQ~~Y~~MHV~~G~~SCQHLSSSAEELR**KARSNSTLSKSEYMVIEE**GGMNHSAF**PQTP**FKTG~~N~~STATCTTNNPNPNSCVNIKKI**FTDV**
 ΔC: NFN~~Y~~F~~Y~~HRET
 Δ1: NFN~~Y~~F~~Y~~HRETEGEEQSQ~~Y~~MHV~~G~~SCQHLSSSAEEL
 Δ2: NFN~~Y~~F~~Y~~HRETEGEEQSQ~~Y~~MHV~~G~~SCQHLSSSAEELR**KARSNSTLSKSEYMVIEE**GG
 Δ3: NFN~~Y~~F~~Y~~HRETEGEEQSQ~~Y~~MHV~~G~~SCQHLSSSAEELR**KARSNSTLSKSEYMVIEE**GGMNHSAF**PQTP**
 ΔSH3: NFN~~Y~~F~~Y~~HRETEGEEQSQ~~Y~~MHV~~G~~SCQHLSSSAEELR**KARSNSTLSKSEYMVIEE**GGMNHSAF**GQTG**FKTG~~N~~STATCTTNNPNPNSCVNIKKI**FTDV**
 ΔPDZ: NFN~~Y~~F~~Y~~HRETEGEEQSQ~~Y~~MHV~~G~~SCQHLSSSAEELR**KARSNSTLSKSEYMVIEE**GGMNHSAF**PQTP**FKTG~~N~~STATCTTNNPNPNSCVNIKKI**WSGG**

Figure 2. Scheme of wild-type Kv1.3 channel and C-terminal mutations. **A)** Alignment of Kv1.2 cortactin-binding site to Kv1.3 C-terminus. **B)** Schematic representation of wild type (WT) Kv1.3 pore-forming alpha subunit with EGFP tag, cortactin-, SH3-, and PDZ-binding regions. **c)** Amino acid sequences of WT Kv1.3 and mutant Kv1.3 C-terminuses starting at amino acid 431. ΔC truncation removes the entire C-terminus except HRET sequence needed for membrane targeting. Δ1 mutation represents truncation of Kv1.3 C-terminus before the predicted cortactin-binding site. Δ2 mutant represents truncation of Kv1.3 C-terminus directly after the putative cortactin binding site. Δ3 mutant represents mutation of Kv1.3 C-terminus directly after SH3 binding site. ΔSH3 mutant represents an amino acid sequence change from PQTP to GQTG. ΔPDZ mutant represents an amino acid sequence change from FTDV to WSGG. Amino acids are listed by their one letter designations.

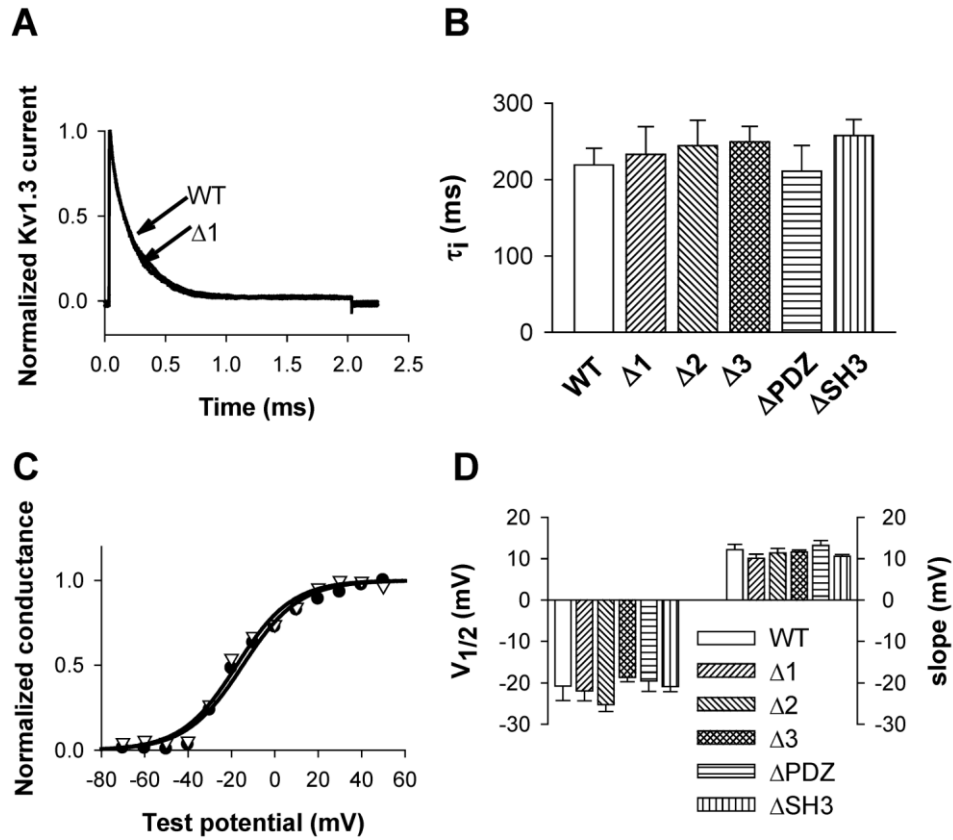


Figure 3. Biophysical characterization of Kv1.3 constructs. **A)** To determine the inactivation kinetics of the currents outside-out patches were depolarized to +40 mV for 2 seconds from a HP of -120 mV. Typical current records for the EGFP-tagged WT and $\Delta 1$ construct are shown. **B)** Average inactivation time constant (τ_i) for various Kv1.3 mutants. **C)** Voltage-dependence of steady-state activation of the Kv1.3 channels in HEK-293 cells, outside-out configuration. The normalized conductance-test potential relationships were recorded and evaluated as detailed in the *Materials and Methods*. Normalized conductance as a function of the test potential for WT (filled circles) and $\Delta 1$ (empty triangles) along with fitted Boltzmann-function (solid lines) are plotted for two actual patches. **D)** Parameters of steady-state activation (slope, k, and midpoint, $V_{1/2}$) are shown for all constructs. The data in B and D are reported as mean \pm SEM of 5-11 cells.

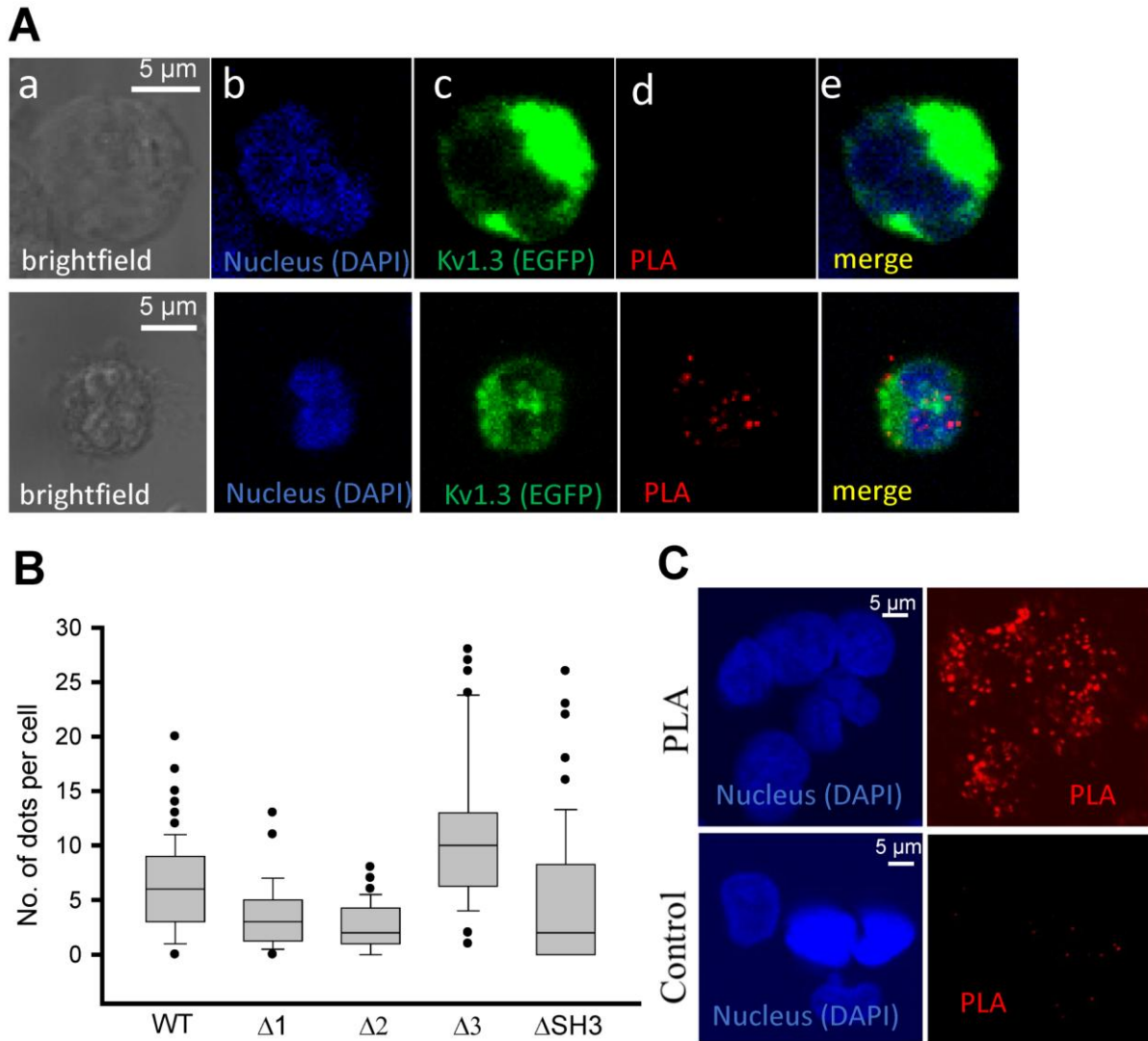


Figure 4. Cortactin and Kv1.3 channel interaction in HEK-293 cells. (A) PLA experiments performed with wild-type, EGFP-Kv1.3-transfected HEK-293 cells. Top row: negative control, only secondary antibodies were added, bottom row: both primary (anti-GFP and anti-cortactin) and secondary antibodies were used. Single protein interactions are visualized as fluorescent red dots. (B) Box plot of number of PLA dots per cell. The data are reported as median, first (top box) and third quartiles (bottom box), and maximum and minimum of 93 cells for WT, 44 for $\Delta 1$, 34 for $\Delta 2$, 60 for $\Delta 3$ and 78 for $\Delta SH3$. All the groups are significantly different from each other ($p < 0.001$) except $\Delta SH3$ vs $\Delta 2$. (C) Interaction between actin and cortactin in HEK-293 cells. HEK-293 cells were labeled with (top row) or without (bottom row, only PLA antibodies) rabbit anti-human cortactin and mouse anti-human actin antibodies, then PLA probe-ligated secondary antibodies were added and PLA was performed according to the manufacturer's protocol. Nuclear staining (DAPI, blue) and PLA signal (red). Scale bar = 5 μm

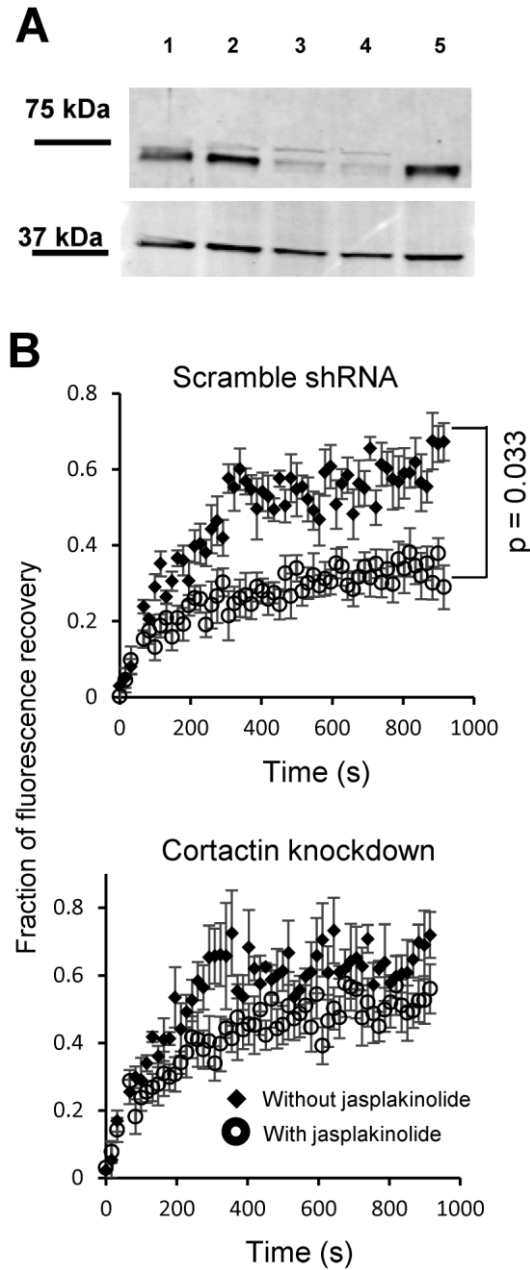


Figure 6. Cortactin knock-down annuls the effect of jasplakinolide. **A)** Western blot of total cell lysates of HEK-293 cells transduced with cortactin or scramble shRNA virus particles using cortactin antibody (1,2: scramble shRNA; 3,4: cortactin shRNA, 5: non-transduced HEK-293). 20 ug of protein lysate was loaded in each lane and the transferred proteins were probed with rabbit anti-cortactin antibody, whereas mouse anti- β -actin was used as a loading control. **B)** Averaged FRAP recovery curves of Kv1.3 wild type channel in cortactin altered HEK-293 cells. Each panel depicts the percent of fluorescent signal recovery at each time point averaged over all FRAP experiments for wild-type Kv1.3 channels with or without cortactin knockdown. Plotted curves include experiments both without jasplakinolide pre-treatment (\blacklozenge) and with jasplakinolide pre-treatment (\circ). Error bars represent the standard error of these averages at each time point (n

= 4-5). Mobile fraction differences with p-values < 0.05 between trials with and without jasplakinolide pre-treatment are listed on the individual graphs.

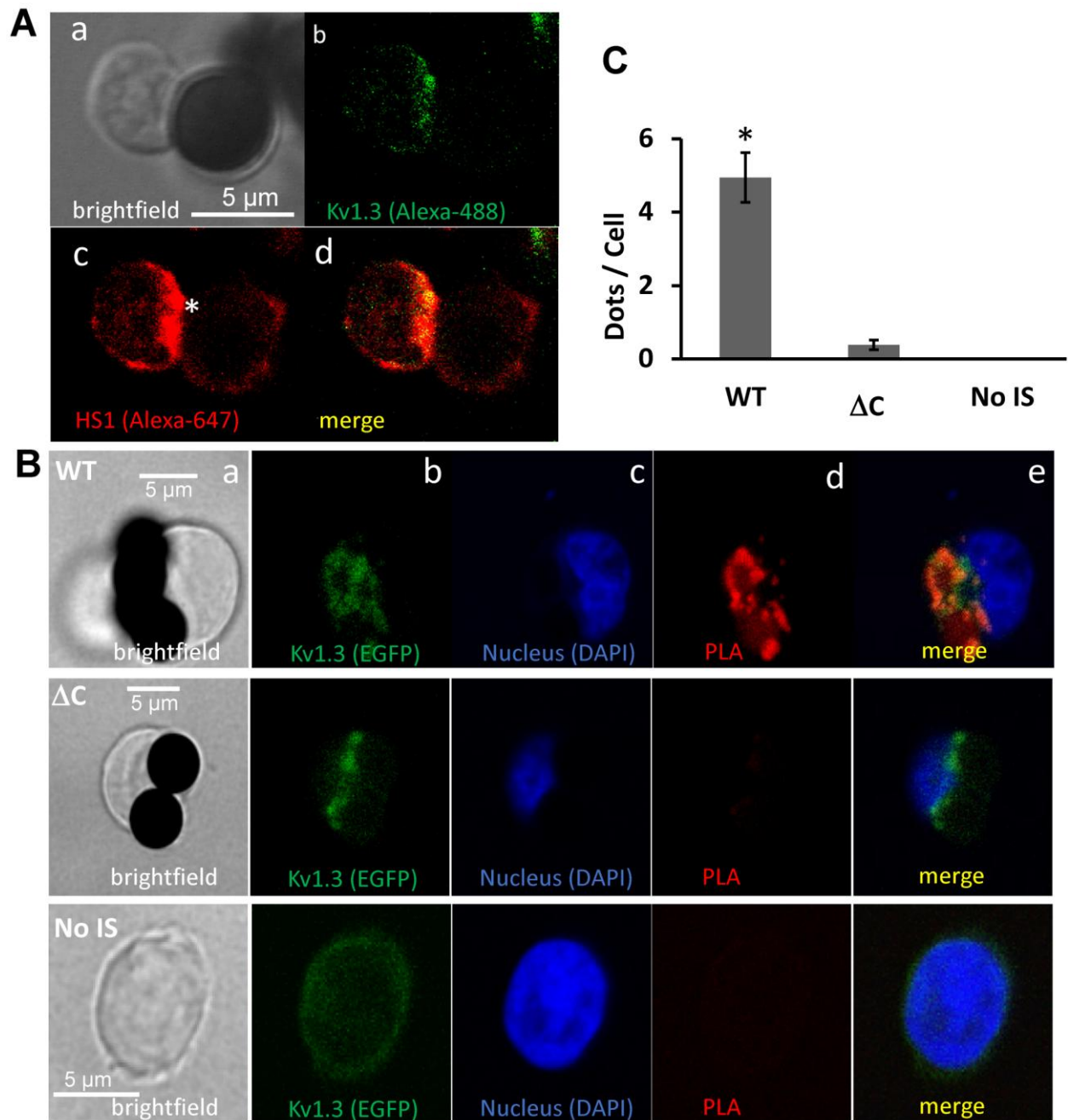


Figure 7. HS1 and Kv1.3 interact at the immunological synapse. B) Micrographs (1 μ m slice size) of human primary T cells forming immunological synapses (denoted with an asterisk in panel c) with CD3/CD28 bead at 30 min. Panels show: a) brightfield, b) Kv1.3 (green), c) HS1 (red), d) merge of green and red channels. The yellow color denotes co-localization of Kv1.3 and HS1. B) Confocal images of representative cells from PLA experiments performed in Jurkat cells stably expressing wild-type mGFP-Kv1.3 channels (WT, top row) and mGFP-Kv1.3 channels with a C terminal truncation (Δ C, middle row) forming immunological synapses with CD3/CD28 beads at 30 min. Jurkat cells overexpressing WT mGFP-Kv1.3 without beads (no IS) are shown

in the, bottom row. Single protein interactions are visualized as red fluorescence dots. (B) Average PLA signals. PLA signals were quantified in cells as number of dots/cell and are represented as mean \pm SEM for 53 cells for WT, 86 for ΔC and 91 for resting, “no IS”, cells. Statistically significant difference was observed in WT vs ΔC and WT vs “no IS” groups ($p < 0.05$), whereas no significant difference was observed between the ΔC and “no IS” groups.

Supplemental Materials

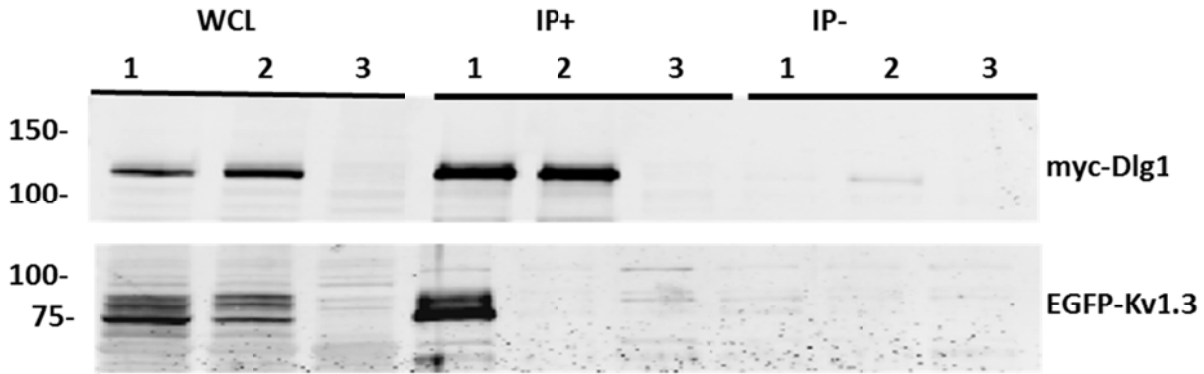
Molecular Biology of the Cell

Hajdu et al.

SUPPLEMENTAL MATERIAL

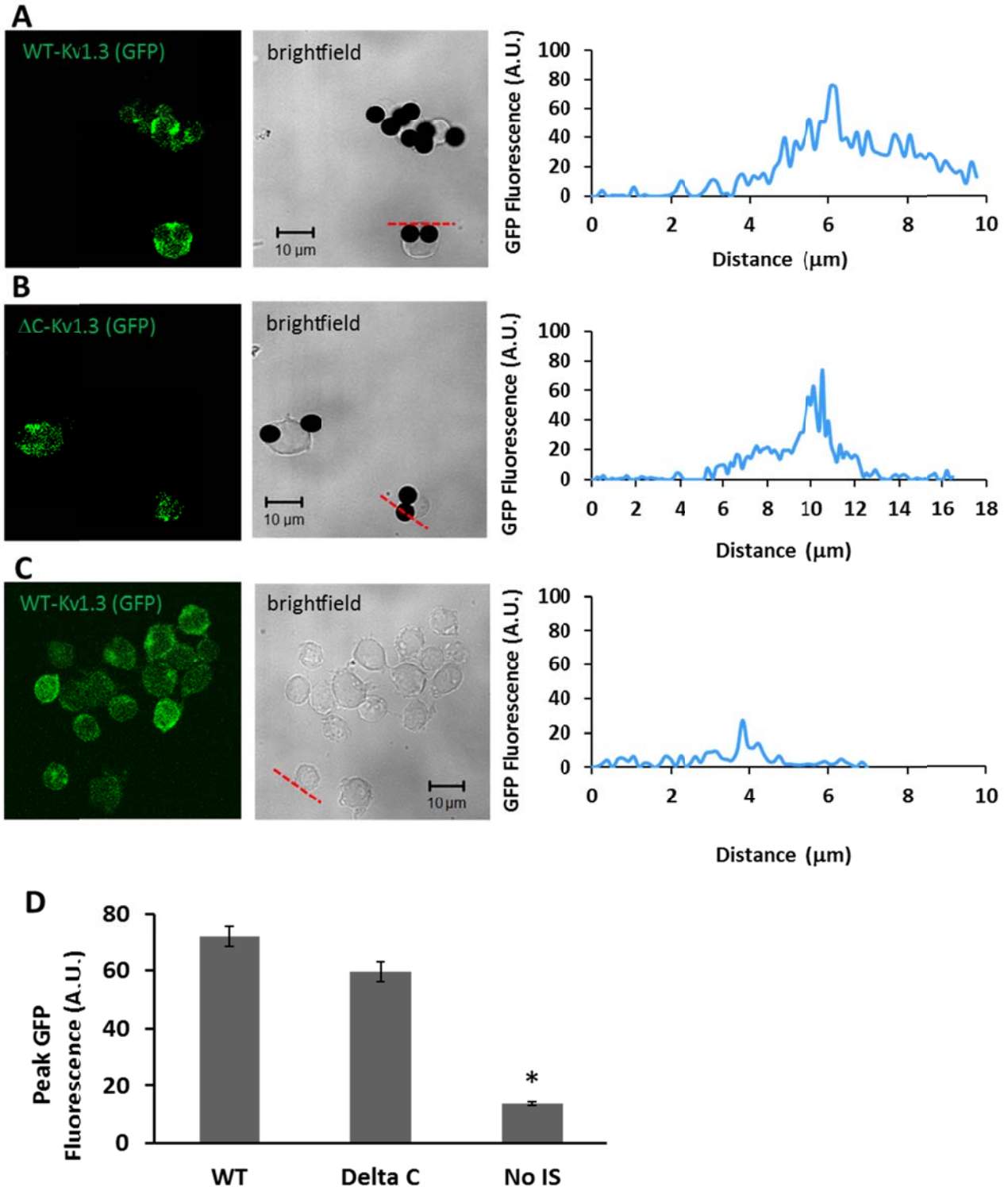
Supplemental Information 1: Immunoprecipitation of Kv1.3 and Dlg-1. HEK-293 cells were transiently transfected by Lipofectamine-2000 (Invitrogen Corp. Life Technologies) with either EGFP-tagged WT Kv1.3 or Δ PDZ and myc-Dlg1 (gift of R.J. Xavier, Harvard Medical School, Boston) plasmid DNAs. Total cell lysate was prepared as previously described (Szigligeti *et al.*, 2006). After centrifugation for 10 min at 1400 rpm at 4°C, the cell pellet was lysed with Pierce[®] IP lysis buffer (Pierce ThermoFisher Scientific) and sonicated for 30 sec. After centrifugation for 10 min at @ 14000rpm and at 4°C, the supernatant was pre-cleared with protein G sepharose beads (Upstate Biotechnology) for 1 hour at 4° C. Beads were removed by centrifugation @ 14000 rpm for 10 min at 4° C and protein content in the supernatant was measured using the Pierce BCA Protein Assay (Thermo Fisher Scientific). Immunoprecipitation was performed for myc-Dlg1 with Pierce c-Myc Tag IP/Co-IP Kit (ThermoFisher Scientific) according to manufacturer's instructions. 600 µg of the pre-cleared lysate was immunoprecipitated by overnight incubation with 10 µl pre-washed anti-c-Myc agarose slurry (5 µg anti-c-Myc antibody). Protein G agarose beads were used as negative control. Beads were thoroughly washed and proteins were eluted from the resin/beads by boiling for 5 min in SDS sample buffer. Western blotting was performed on the eluted proteins as described in Materials and Methods and the proteins were probed with mouse anti-c-Myc (1:800 fold, Covance) and rabbit anti-GFP (1: 100 fold, Santa Cruz Biotechnology Inc) primary antibodies and Alexa Fluor 680 anti-rabbit and IRDye 800CW anti-mouse secondary antibodies. The blots were subsequently visualized on LI-COR Odyssey[®] infrared scanner and analyzed using Odyssey v3.0 software as described earlier.

Supplemental Information 2: Immunological Synapse Quantification. Experiments were conducted to establish that an IS with Kv1.3 accumulation was formed at the T cell-beads point of contacts. Confocal images obtained for Jurkat T cells in PLA experiments were quantitated for GFP fluorescence in the presence or absence of CD3/CD28 beads using Image J. Using the line selection tool, lines were drawn either in the region of contact between an individual cell and beads or along the cell membrane, not in contact with the beads (resting, "No IS"). GFP fluorescence was measured using the "Plot Profile" tool. The peak green fluorescence intensity was comparable in WT and Δ C Kv1.3-expressing cells and significantly higher than resting (no beads/no IS) WT-Kv1.3 Jurkat cells (Supplemental Figure 2).



HEK 293	1	2	3
myc-dlg1	+	+	-
Wt-Kv1.3	+	-	-
Δ PDZ-Kv1.3	-	+	-

Supplemental Figure 1. The Δ PDZ Kv1.3 mutant lacks the ability to bind Dlg1. Western blot depicts immunoprecipitation of myc-Dlg1 with wild-type EGFP-tagged Kv1.3 channel but not Δ PDZ mutant Kv1.3. HEK-293 cells were co-transfected with myc-Dlg1 along with either wild-type EGFP-Kv1.3 (column 1), Δ PDZ mutant with EGFP (column 2) or neither (column 3). 600 ug of pre-cleared protein lysate were immunoprecipitated with 5 ug of anti-myc antibody (IP+) or Protein G sepharose beads (IP-) and were run on a Tris-Glycine gel along with 40 ug whole cell lysates (WCL). Western Blotting was performed and the blots were probed with either mouse anti-myc or rabbit anti GFP antibodies (see *Supplemental Information 1* for the detailed procedure and antibody concentrations).



Supplemental Figure 2: Kv1.3 channel localization in the immunological synapse: Confocal microscopy images of Jurkat T cells stably expressing either mGFP tagged wild-type Kv1.3 channels (WT, A) or mGFP-Kv1.3 channels with a truncated C terminus (Δ C, B) forming immunological synapse with CD3/CD28 beads at 30 min. Jurkat cells stably expressing wild-

type mGFP Kv1.3 channels incubated without the beads (no IS) are shown in C. GFP fluorescence was quantified along a line drawn either in the region of contact with the beads or randomly along the plasma membrane for resting (no bead/no IS) cells (shown in the brightfield image) and the values of the corresponding GFP fluorescence are shown in the right panels. (D) Average peak mGFP fluorescence for 31 cells for WT, 23 cells for ΔC and 27 cells for “no IS” ($p < 0.001$).